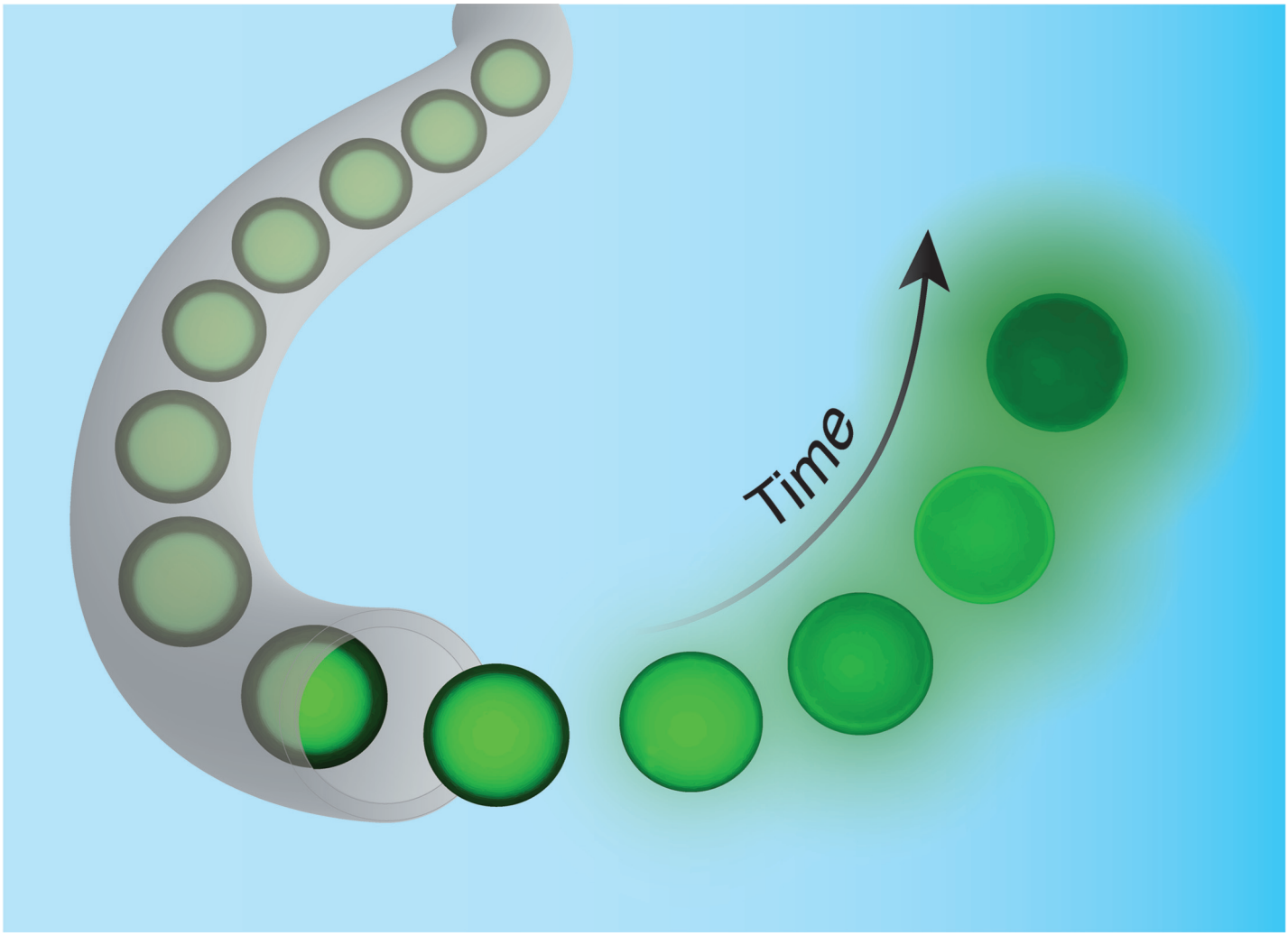


**Highlighting work performed at the DWI-Leibniz Institute for Interactive Materials in Aachen, Germany.**

Microfluidic fabrication of polyethylene glycol microgel capsules with tailored properties for the delivery of biomolecules

Microgel capsules loaded with fluorescently labeled dextran are produced *via* photo-polymerization inside a microfluidic device.

## As featured in:


See Alexander J. C. Kuehne, Laura De Laporte *et al.*, *Biomater. Sci.*, 2017, **5**, 1549.

ROYAL SOCIETY OF CHEMISTRY

rsc.li/biomaterials-science

Registered charity number: 207890

Biomaterials Science

PAPER

View Article Online
View Journal | View Issue



Cite this: *Biomater. Sci.*, 2017, **5**, 1549

# Microfluidic fabrication of polyethylene glycol microgel capsules with tailored properties for the delivery of biomolecules†

Luis P. B. Guerzoni, ‡ Jan Bohl, ‡ Alexander Jans, Jonas C. Rose, Jens Koehler, Alexander J. C. Kuehne * and Laura De Laporte *

Received 10th April 2017,
Accepted 20th May 2017

DOI: 10.1039/c7bm00322f

rsc.li/biomaterials-science

Microfluidic encapsulation platforms have great potential not only in pharmaceutical applications but also in the consumer products industry. Droplet-based microfluidics is increasingly used for the production of monodisperse polymer microcapsules for biomedical applications. In this work, a microfluidic technique is developed for the fabrication of monodisperse double emulsion droplets, where the shell is crosslinked into microgel capsules. A six-armed acrylated star-shaped poly(ethylene oxide-*stat*-propylene oxide) pre-polymer is used to form the microgel shell after a photo-initiated crosslinking reaction. The synthesized microgel capsules are hollow, enabling direct encapsulation of large amounts of multiple biomolecules with the inner aqueous phase completely engulfed inside the double emulsion droplets. The shell thickness and overall microgel sizes can be controlled *via* the flow rates. The morphology and size of the shells are characterized by cryo-SEM. The encapsulation and retention of 10 kDa FITC-dextran and its microgel degradation mediated release are monitored by fluorescence microscopy.



## Introduction

Advanced drug delivery systems (DDS) show great potential to improve the efficacy of common drug therapies. As in systemic applications (*e.g.*, orally in the form of pills), the pharmaceutically active compound is often metabolized directly after application,[1] and DDS have been developed to alter and improve the pharmacokinetics and bio-distribution of the loaded drug.[2] By incorporating specific binding ligands, targeted drug delivery becomes possible, reducing unwanted side effects, thus allowing the application of higher doses. At present, most of the FDA approved DDS are based on polymer–drug conjugates (Omontys®), liposomes or micelles (DepoDur®, AmBisome®, Doxyl/Caelix® and DepoCyt®), biodegradable carriers like poly(lactic-*co*-glycolic acid) (Ozudex®), or proteins, such as monoclonal antibodies (Brentuximab®).[1,2] Polymers have also been applied to fabricate solid nano- and microspheres,[3,4] microcapsules,[5] or nano-[6] and microgels[7] to temporally and spatially control drug delivery. Microcapsules with a solid polymer shell are significantly more stable compared to micelles or liposomes. In addition, they have a large internal volume, which can be loaded directly during capsule formation. Due to these beneficial properties, they represent promising vehicles for targeted delivery and release of compounds, not only as DDS in medicine but also in cosmetics and food applications.[8]

In contrast to solid particles and capsules, polymers can be crosslinked to form hydrogels. Hydrogels can be swollen with water at high volume fractions, depending on their crosslinking density.[9–11] When such materials are produced with nano- to micrometer dimensions, they are termed microgels. These soft microgels represent ideal carrier entities for DDSs, as they exhibit unique properties in comparison with hard polymer carriers. The high surface to volume ratio of the polymer network enables them to entrap a large amount of therapeutic molecules, such as carbohydrates,[12] proteins[7] and DNA,[13] which can be loaded *via* covalent[14] or supramolecular binding.[15] In addition, the incorporation of inorganic species, such as quantum dots and magnetic nanoparticles has also been reported.[16–18] The microgels can also be modified with recognition ligands to target specific tissues[19,20] and their chemistry can be fine-tuned to control the release mechanism and kinetics of the loaded drugs.[21] Furthermore, the porous network structure enables diffusion-controlled release of small molecules, which can be further tailored when using degradable microgel networks. The *in vitro* release kinetics of bioactive compounds from hydrogel networks has been extensively investigated.[22–24]

*DWI Leibniz Institute for Interactive Materials, Forckenbeckstrasse 50, Aachen, Germany. E-mail: kuehne@dwi.rwth-aachen.de, delaporte@dwi.rwth-aachen.de*

† Electronic supplementary information (ESI) available: Additional experimental data of the synthesis and analysis of star-shaped PEG-acrylate and movies of the W/O/W double emulsion formation in the microfluidic device and dried microgel capsules swelling in water. See DOI: 10.1039/c7bm00322f

‡ These authors contributed equally to this work.

Depending on the fabrication method, the size of the microgels can be modulated. Standard bulk emulsification or precipitation is mostly applied, resulting in nano- and microgels with diameters in the range of 100 nm to 10 μm.[6,25,26] Here, drugs can be loaded during microgel preparation[6] or bound to the network post production *via* diffusion or coupling.[14,27] One of the main challenges here is efficient loading of the drug. Loading by diffusion results in a large fraction of the drug remaining in the dispersion medium, often leading to high losses and increased costs. In addition, emulsions produced by stirring result in polydisperse samples with limited control over the essential physical and mechanical particle properties, such as the mesh size and dimensions.[28] These inhomogeneities impede precise temporal control over the release kinetics of the drug molecule.

To better control the release kinetics, core–shell or hollow microgels have been established to entrap the drugs inside the lumen and control their release *via* the properties of the shell. The most common method to produce these microgel architectures is to apply a template, around which a shell is formed.[29] For these geometries, we can envision only two approaches for loading of drugs into these soft containers: either the drug is already pre-loaded in the template, or the template is dissolved and the hollow lumen is filled with drugs *via* diffusion. The disadvantage of both approaches remains the low encapsulation efficiency and insufficient control over the release. To improve this, hollow PNIPAM nanogels have been produced by sequentially crosslinking PNIPAM and poly(*N*-isopropyl metharcylamide) (PNIPMAM) around silica particles, which can dissolve post fabrication.[30] As both PNIPAM and PNIPMAM shells have different lower critical solution temperatures (LCSTs) of 32 and 42 °C, respectively, they have the ability to load drugs inside *via* diffusion when both shells are swollen, while the drugs can be entrapped in the cavity when the temperature is increased between both LCSTs, resulting in a collapse of the inner shell. Here, the drugs are still loaded post fabrication, and the microgels are produced in batch, which may lead to heterogeneous microgel properties.

To produce monodisperse microgels, enhance the encapsulation efficiency, and control their physical and mechanical properties, microfluidic techniques are applied where microgels are prepared in confined volumes.[31–33] Standard (single emulsion) microfluidic dropmakers have been used for the production of monodisperse particles and microgels from the nano- to the microscale.[34,35] Inside the microchannels, interfacial and viscous forces dominate over bulk forces and the droplet formation dynamics can be controlled by parameters, such as the flow rates of the fluids, their viscosities, interfacial tension, densities, surface chemistry, and channel geometry.[36] After a microgel precursor-carrying phase is emulsified by an immiscible continuous phase, polymerization and/or crosslinking can be triggered inside the droplets to produce droplet-templated microgels.[35,37] Using microfluidics for loading active compounds inside the microgels represents a formidable technique to circumvent the above described problems of diffusive loading or loading *via* a carrier. However, these microgel architectures remain limited in their capacity and temporal control of the release. For example, dextran-loaded core–shell microgels consisting of a polyacrylamide core and a PNIPAM shell have been produced *via* microfluidics.[33] This approach is, however, still restricted, as it requires two polymer components, and limited, as the core of the particle is occupied by microgels.

On the other hand, droplet-based microfluidic techniques can be applied to form double emulsions with high precision and exquisite control over the number and size of the core droplets.[28,38] This method enables direct loading of a large concentration of drugs inside the lumen and crosslinking of a second phase to form a protective shell, which can retain the drugs and control its release.[21,39] Currently, double emulsion microfluidics has only been applied to make DDS with solid shells, which release the drug upon breaking. For example, solid microcapsules can be produced using acrylate based monomers, which are cured using a UV initiated crosslinking reaction.[8] However, the degradation products are not biocompatible, obviating their application in biological environments.[40,41] A biocompatible approach was realized by using polycaprolactone as the capsule shell material, in which proteins were encapsulated.[42] While these approaches are promising in terms of shelf-life, it remains difficult to trigger and control the release of the active compound.

To circumvent the above described problems, a DDS system would ideally be loaded during microfluidic production and consist of a soft and responsive shell. The absence of such a system prevents the translation of high capacity drug carriers into clinical applications. While there are a variety of suitable hydrogel materials available[11,43–48] with adjustable mechanical, chemical, and physical properties, there remains a lack of suitable microgel capsule approaches for DDS applications.

In this present study, we develop a double emulsion microfluidic method to produce microgel capsules, where we directly load bioactive molecules inside the cavity during the formation of the microcapsule. The shell is formed by crosslinking 20% (w/w) six-armed acrylated star-shaped poly(ethylene oxide-*stat*-propylene oxide) using a biocompatible photoinitiator with absorption in the UV region. This results in capsules with a soft microgel shell, which can respond to their environment *via* hydrolysis to facilitate controlled drug release. Bulk hydrogels made with the same polymer composition have previously been reported to have an elastic modulus of approximately 3100 Pa, a swelling degree of about 280%, and a theoretically calculated mesh size of 2.5 nm.[18,49] In addition, these hydrogels have been shown to be non-cytotoxic.[18,50] As the shell degrades by breaking the ester bonds, no toxic free acrylates are present in the degradation products. The microfluidic technique applied here allows production of PEG-based microgel capsules with tunable dimensions, shell thickness and density, and degradation rate. We demonstrate the retention and release of fluorescently labelled dextran (MW = 10 kDa) as a proxy for an active component. As we apply a molecularly defined pre-polymer to produce the microgel shell, we have the opportunity to provide a platform of microgel capsules

 

with tailored properties that can precisely control the release kinetics in a temporal manner, depending on the desired application. The microgel capsules reported here can be directly loaded with high concentrations of bioactive molecules during their microfluidic generation. The capsules have the potential for controlled release, while the kinetics can be tuned by varying the properties of the synthetic hydrogel shell. The capsules can be produced with tailored dimensions and shell thickness, and are synthesized in a monodisperse manner due to the microfluidic fabrication method.

## Results and discussion

To form the microfluidic reactor, we use glass capillary technology, where tapered capillaries with a round cross-section are aligned inside a square capillary with an inner diameter slightly larger than the outer diameter of the round glass capillaries, using established protocols (see Fig. 1B).[51] (The diameters of the tapered orifices of the small and big round capillaries are between 50 and 60 μm and between 200 and 225 μm, respectively, the inner diameter of the square capillary is 205 μm, and the distance between the two tapered orifices is between 50 and 110 μm.) We produce water-in-oil-in-water (W/O/W) emulsions by connecting the respective liquids to the dedicated inlets of the device and we drive the liquids using syringe pumps. The inner, middle, and outer phases are composed of PBS with 2% (w/w) Tween 80, toluene with 5% (w/w) Span 80, and water with 2% (w/w) Tween 80, respectively. To the middle toluene phase, we add an acrylate-functionalized six-armed star-shaped poly(ethylene oxide-*stat*-propylene oxide) (sPEG-A) pre-polymer with a molecular weight of 3 kDa. We also admix a radical photoinitiator (9% (w/w) Irgacure® 1173), which is activated by exposure to a UV emitting lamp ($\lambda_{em}$ = 254/366 nm) (Fig. 1A and B). Movie 1 in the ESI† shows the microfluidic device producing W/O/W double emulsions that are crosslinked downstream.

We manipulate the double emulsion formation by fixing the flow rates of the outer phase ($Q_o$) at 10 mL $h^{-1}$ and the middle phase ($Q_m$) at 2 mL $h^{-1}$, and varying the flow rate of the inner phase ($Q_i$). With these settings, we can modify the oil shell thickness of the formed double emulsion droplets while maintaining the overall double emulsion size relatively constant. To investigate these conditions, we use two fluidic

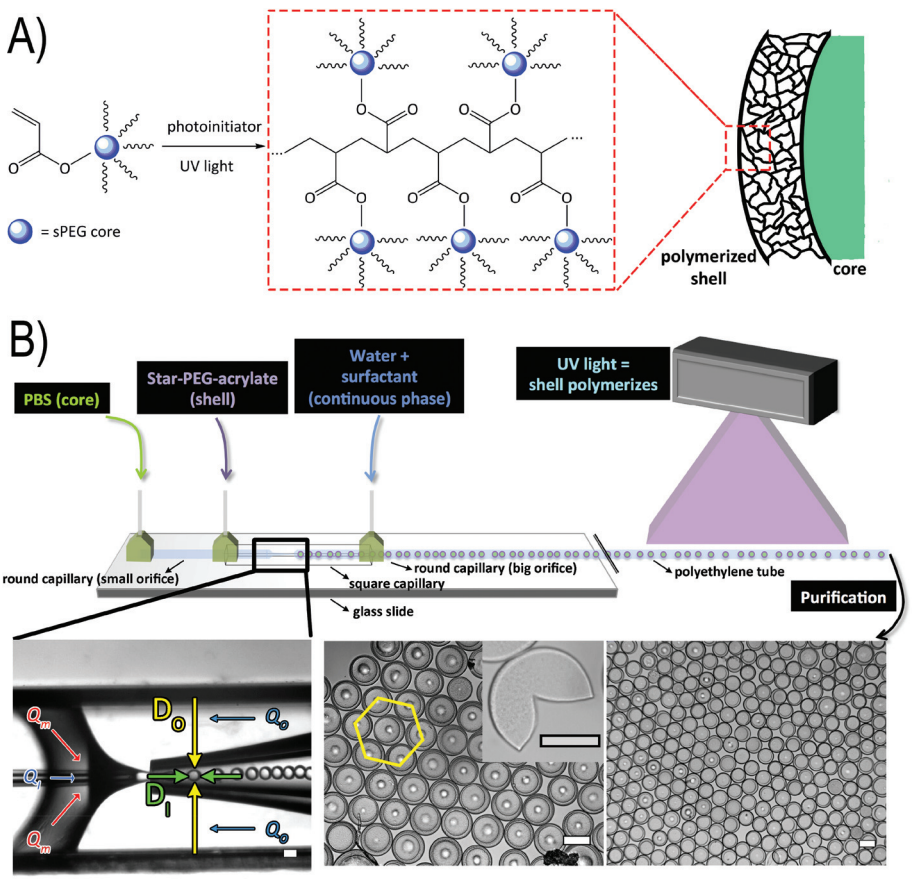


**Fig. 1** (A) Schematic of the chemical crosslinking process of the sPEG-A. (B) The experimental set-up: two round capillaries are placed inside a square capillary. The injection of the respective liquids allows the formation of double emulsions where the capillaries are aligned. After double emulsion formation, a UV light illuminates the double emulsion droplets for 5–15 seconds to polymerize the sPEG-A and produce microgel capsules. White dots inside microgel capsules appear due to contact with the glass slide at their bottom. Scale bars are 100 μm.

systems: a model fluidic system consisting of the aforementioned liquid phases in the absence of pre-polymer, and a system containing a non-reactive sPEG-OH pre-polymer (MW = 3 kDa) to simulate the viscosity of the real sPEG-A loaded oil phase we apply further. Upon decreasing $Q_i$ from 2 mL $h^{-1}$ to 1 mL $h^{-1}$, the shell thickness of the model fluidic system double emulsions increases from 10.5 to 17.3 μm, while the overall droplet size remains relatively constant (see Fig. 2A). When using the non-reactive pre-polymer solution, the increased viscosity (2.224 mPa s *versus* the pre-polymer free solution at 0.664 mPa s) leads to a shell thickness window of 9.9 to 18.9 μm. The shell thickness ($Ø_{shell}$) of the double emulsion droplets is determined by measuring the outer diameter of the droplet ($D_o$), subtracting the diameter of the inner droplet ($D_i$), and dividing this value by half. Similar ranges of flow rates have been reported before.[52]

In a second experiment to control the droplet dimensions, a glass capillary device is used where the outer flow rate ($Q_o$) is varied, while keeping the middle ($Q_m$) and inner ($Q_i$) flow rates constant at 4 and 1.5 mL $h^{-1}$, respectively. With this configuration, we are able to tune the overall droplet size (from 178.6 to 210.0 μm) while maintaining the shell thickness constant (see Fig. 2B). Reducing the flow rates by half while keeping their ratio constant leads to an unstable system, which does not produce double emulsion droplets. In addition, higher flow rates result in jet formation and downstream turbulences, also forbidding the generation of monodisperse double emulsion droplets.

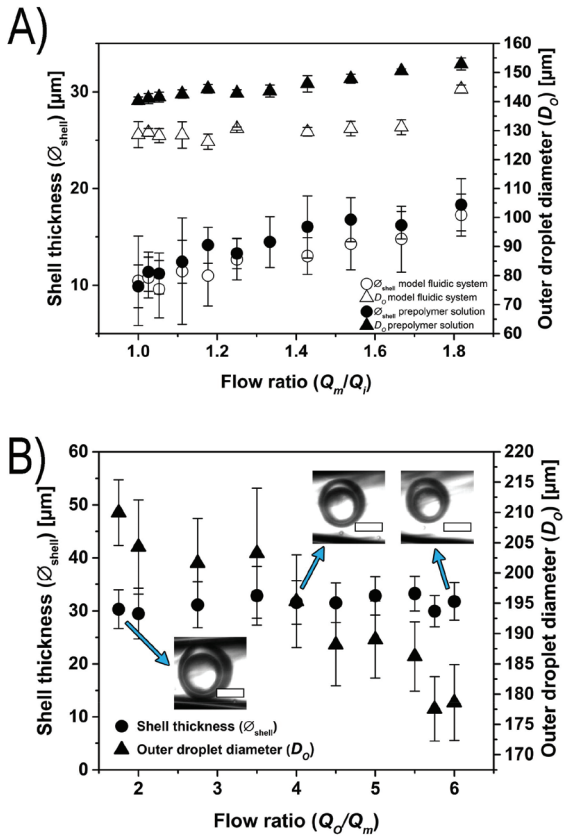


Fig. 2 (A) The variation in shell thickness: tuning of the flow rates allows precise control over the shell thickness while maintaining the outer diameter. The outer ($Q_o$) and middle ($Q_m$) flow rates are kept constant at 10 and 2 mL $h^{-1}$, respectively. (B) The variation in droplet dimensions: tuning of the flow rates allows precise control over the outer diameter while maintaining the shell thickness. Here, the outer, middle and inner phases are composed of water with 1% (w/w) Tween 80, toluene with 10% (w/w) non-reactive sPEG and PBS. The middle ($Q_m$) and inner ($Q_i$) flow rates are kept constant at 4 and 1.5 mL $h^{-1}$, respectively. Scale bars are 100 μm.

After successfully demonstrating the formation of double emulsion droplets, and the ability to control their size and shell thickness, the middle fluidic phase is exchanged to the reactive sPEG-A pre-polymer solution to generate microgel capsules. This pre-polymer solution contains 20% (w/w) sPEG-A and 9% (w/w) Irgacure® 1173 in toluene. A UV emitting lamp ($\lambda_{em}$ = 254/366 nm) is applied for crosslinking to allow complete polymerization of the microgels within the short residence time in the microfluidic device. The double emulsion droplets are polymerized downstream in the tubing guiding the double emulsion away from the microfluidic chip. The obtained crosslinked monodisperse microgel capsules are shown in Fig. 1B. Small dots in the center of microgels appear due to their contact with the glass slide.

The microgel capsules are sequentially purified by evaporation of toluene and washing with water, isopropanol, and 1× PBS to remove traces of toluene and excess surfactant. After collection, the microgel capsules cream due to the low density of the remaining toluene in the middle phase. Upon removal of the toluene the microgels settle to the bottom of the collection vial over the course of 9 days (Fig. 3A). The purification is done in a much shorter time frame of approximately 1 hour *via* multiple centrifugation steps, after which the microgel capsules are still stable and remain monodisperse, as shown in Fig. 1B. The microgel capsules are stored at 5 °C and show no change in their macroscopic structure over the course of at least two weeks. To minimize microgel attachment to the inner surface of the tubing, low protein binding tubes are used. The robustness of the microgel capsules is verified by centrifugation at 12 000 rpm for 20 minutes, after which the majority of the microgel capsules remain intact. Unlike solid capsules, the microgel capsules are also resistant towards sonication at 120 W. Only with the application of strong mechanical stress, for example by pressing two glass slides together, the microgel capsules break (Fig. 1B, inset).

To determine the degree of swelling, the microgel capsules are dried and then again dissolved in water. The shell diameter is monitored over time upon swelling (see Fig. 3B). As the dried microgel capsules stick to the glass surface, they tend to flatten. The resulting oblate shape can be compared to the form of a red blood cell. During re-swelling, the microgel capsules show a fast increase in their diameters during the first thirty seconds. This steep increase is caused by the uptake of water molecules due to the hydrophilic character of the PEG shells[53] and represents the fast uptake of total bound water. Water then infuses into the meshes of the hydrogel due to

 

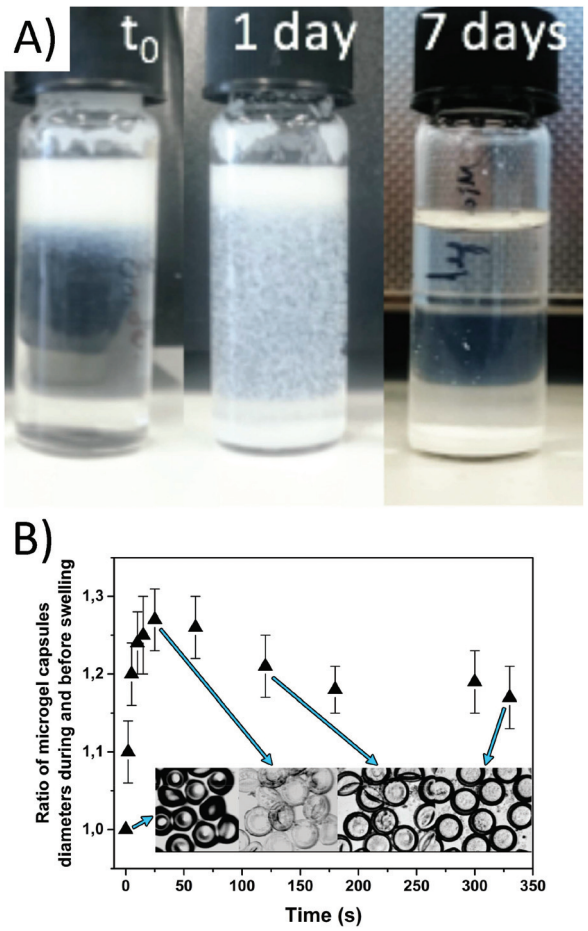


Fig. 3 Swelling behavior of the sPEG microgel capsules: (A) the exchange of toluene for water in the microgel shell over time. The creamed capsules sediment after the toluene is evaporated over the course of 9 days. (B) Swelling experiments of microgel capsules in water. The change of the diameter is recorded over time. The dried oblate particles swell rapidly.

osmotic pressure, swelling the shell to its maximum, which is reached when the polymer chains attain their maximum extension lengths. This fast process is followed by water slowly migrating through the hydrogel network to fill up the inner hollow core of the microgels. In this case, no molecular interactions enhance the process and therefore the migration is slow compared to the first swelling. After 30 seconds, a slow decrease in the diameter of the microgel capsules is observed, as the microgels transition from a flat oblate shape to 3D spherical microgel capsules. This process can be observed in Fig. 3B, and in Movie 2 in the ESI.† Between 40 and 330 seconds, the outer diameter of the microgel capsules is increased by 12 μm, enhancing the total diameter by a factor of 1.2.

For more detailed insight into the structure of the microgel capsules, cryo-surface electron microscopy (cryo-SEM) is performed. The advantage of the cryo-SEM technique is that it allows investigating the structure of microgel capsules without altering the native shape and morphology. As a result, the three dimensional structure of the microgel capsules can be imaged as if they are swollen in water. During imaging, the vitrified water can be sublimated, revealing the naked polymer structure (see Fig. 4A and B). The shell thickness after 10 minutes of sublimation varies between 10 and 20 μm for the observed microgel capsules in Fig. 4A, which is consistent with the measured shell thicknesses for microgel capsules in Fig. 2A. The structure of the microgel shell is found to be highly porous. To also visualize the three-dimensional geometry of the microgel capsules, sublimation times are increased to 25 minutes to remove larger parts of the vitrified ice matrix (see Fig. 4C). All three microgels clearly show the empty microcapsule void. The pores in the shell of the microgel capsules appear larger than their real dimensions due to a typical artifact, which occurs during cooling and drying to prepare the sample for SEM imaging. During freezing, ice crystals form in the hydrogel structure, which push away the polymer chains and produce a porous structure. We hypothesize that the polymer strings, visible in the void, result from residual stabilizer or non-crosslinked sPEG-acrylate, as the strings are aligned with the direction of the ice crystals.

To demonstrate the encapsulation capability of the microgel capsules, a 10 kDa fluorescein functionalized (FITC) dextran ($\lambda_{abs}$ = 492 nm, $\lambda_{em}$ = 518 nm) is chosen to serve as a biological proxy. Fluorescently labelled dextran is available in a broad range of molecular weights and is often used to simulate the permeation and diffusion behaviour of biomolecules.[42] 10 kDa FITC-dextran remains inside our microgel capsules after all the previously described purification steps (Fig. 5A and B), proving that the mesh size of the microgel capsule, resulting from crosslinking of the 3 kDa sPEG precursor, is small enough to retain the dextran molecules. The differences in fluorescence intensity of the microgel capsules in Fig. 5B and D are due to the fact that not all microgels are in focus during fluorescence microscopy.

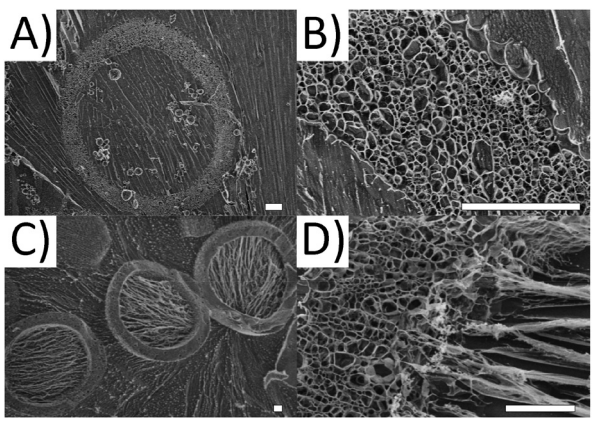


Fig. 4 Cryo-SEM images of the microgel capsules: samples are purified and stored in Milli-Q water. (A) 10 minutes sublimation time at −80 °C, 700×; (B) 10 minutes sublimation time at −80 °C, 5000×; (C) 25 minutes sublimation time at −80 °C, 400×; (D) 25 minutes sublimation time at −80 °C, 3000×. Scale bars are 10 μm.

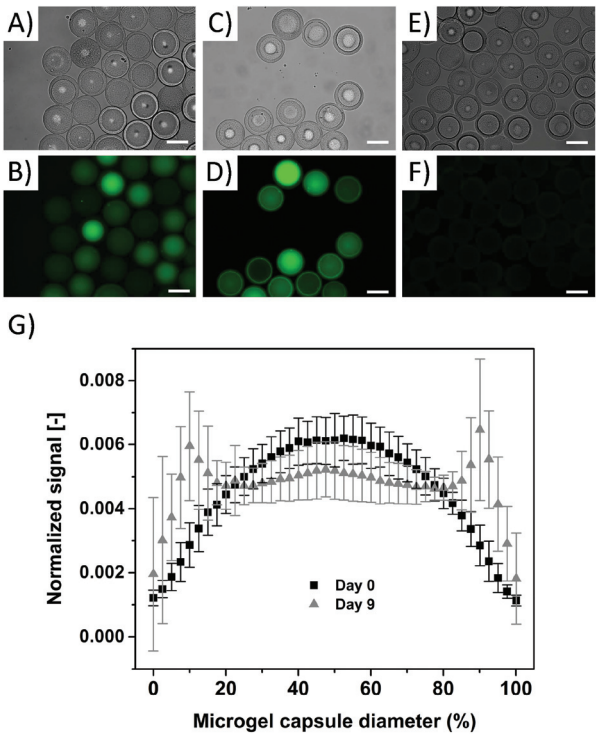


**Fig. 5** Images of microgel capsules: (A–B) containing 0.01% (w/w) encapsulated 10 kDa FITC-dextran immediately after purification (day 0) and (C–D) 9 days after purification. (E–F) Control microgel capsules without FITC-dextran. The first row shows the bright-field images, while the second row portrays the fluorescence images. Dots inside microgel capsules appear due to contact with the glass slide at their bottom. The differences in fluorescence signals can be explained by the different positions of the microgel capsules in the *z*-dimension, resulting in bright signals for microgel capsules, which are in focus with their entire perimeter, and dimmer signals in the case of microgels above or below this focal plane. Scale bars are 100 μm. (G) Fluorescence spectra of dextran across the diameter of the entire microgels, normalized over the total fluorescence signal inside each microgel and the distance from the center of the microgel.

Monitoring the sample over nine days shows that dextran molecules are partly retained inside the microgel capsules, with an increase in fluorescence in the shell after 9 days. This is concomitant with a decrease in the fluorescence in the core, indicating that dextran diffuses through the microgel network, most likely supported by the hydrolysis of the ester bonds present in the hydrogel network[50] (see Fig. 5C and D). In order to analyze the dextran distribution inside the microgel capsules, the distribution of the fluorescence signal intensity is analyzed across their diameter. Here, the fluorescence signal is related to the integral of all signals per microgel capsule, and normalized over the distance from the center of the microgel capsule. These results reveal a clear difference in dextran distribution, with a bell-shaped curve at day 0 and a maximal intensity in the center of the capsule, and two significant peaks at the location of the microgel shell at day 9 (Fig. 5G). This indicates that the generated microgel capsules can be applied to encapsulate biomolecules with size equal to or larger than the tested 10 kDa FITC-dextran with a hydrodynamic radius of 2.36 nm.[54] The versatile fabrication method of the microgel capsules enables loading of differently sized biomolecules and, depending on the polymer composition of the shell, can control the release rate *via* the thickness and density of the shell and the network degradation rate.

## Conclusions

We demonstrate a method for the production of microgel capsules and concomitant loading with biomolecules, actives, or drugs using microfluidics. Biomolecules can be retained by the small network mesh size and are released after hydrolysis of the network. While this study clearly indicates the high potential of microgel capsules for the loading and release of biomolecules, the effect of size dependent diffusion through the microgel network and the contribution of hydrolysis to degrading the molecular network will be further investigated. In the future, such porous microgel capsules with controlled mesh sizes and potential hydrolytic or light-induced degradation will enable precise delivery of actives for drug delivery, agriculture, and cosmetics.

## Experimental section

### Materials

Round capillaries (borosilicate, outer diameter 1.0 mm, inner diameter 0.58 mm, Hilgenberg, Malsfeld, Germany); square capillaries (borosilicate, outer diameter 1.5 mm, inner diameter 1.22 mm, Hilgenberg, Malsfeld, Germany); epoxy resin two-component glue (Wiko, Gluetec, Greußenheim, Germany); a fine bore polyethylene (PE) tube (inner diameter: 0.86 mm, outer diameter: 1.52 mm, Portex, smiths-medical, Minnesota, U.S.A.); trimethoxy(octyl)silane (TMOS) (Sigma-Aldrich, Germany); Microlance 3 (20G × 1″, 0.9 × 25 mm) needles.

### Microfluidic experiments

Six-armed star-shaped poly(ethylene oxide-*stat*-propylene oxide) (sPEG-OH) was synthesized from a sorbitol core with a molecular weight of 3 kDa (CHT R. Beitlich GmbH); sPEG-OH was modified with acrylate groups as described before;[55] fluorescein isothiocyanate–dextran (FTIC-dextran, MW = 10 kDa, TCI); phosphate buffered saline, pH 7.2 (PBS, Lonza); 2-hydroxy-2-methylpropiophenone (Irgacure® 1173, BASF); isopropanol (ACS reagent, $w \geq 99.5$, Sigma-Aldrich); Tween 80 (Sigma-Aldrich); Span 80 (Sigma-Aldrich), toluene ($w$ = 98%, VWR).

### Methods

**Microfluidic device production.** Glass capillary devices are designed according to an adapted version of Utada *et al.*[51] Round glass capillaries are pulled using an electrical capillary puller (PC10, Narishige, Tokyo, Japan). Inlet and outlet capillaries are formed with 1500-grid sandpaper and a micro forge

 

(Micro Forge, MF-900, Narishige, Tokyo, Japan), equipped with a hot platinum wire to shape the edges of the inlets and outlets after grinding. The inlet capillaries are dip-coated in trimethoxy(octyl)silane to render the glass surfaces hydrophobic. After dipping for twenty minutes, excess silane is removed with ethanol and the capillary heated at 80 °C for 30 minutes. To assemble the device, the round capillaries are put into a square capillary and placed on a microscope glass slide. To fix the capillaries and form inlet and outlet holes for the device, syringe needles with openings at their bottom are glued onto the microscope glass slide and the capillaries, applying epoxy-resin two-component glue.

**General workflow for microfluidic devices.** Microfluidic experiments are conducted on a microfluidic system consisting of three syringe pumps (PHD Ultra, Harvard Apparatus, Holiston, U.S.A.), to control the flow rates of the three different phases. An inverted microscope (Motic AE2000, TED PELLA, INC., Redding, CA) equipped with a camera (Flea3, Point Grey, Richmond, CA) is applied to image droplet formation. The glass capillary microfluidic device is connected to the system using fine bore polyethylene tubing (0.86 mm inner diameter, 1.52 mm outer diameter). The following liquid phases shown in Table 1 are used in this project. To save material, the viscosity of the reactive 3 kDa sPEG-A phase is assumed to be similar to that of the non-reactive sPEG-OH at the same concentration.

**On-chip polymerization.** In order to polymerize the shell of the double emulsion droplets, the following middle oil phase is used: 20% (w/w) 6-armed sPEG-A in toluene and 9% (w/w) Irgacure® 1173. The double emulsion droplets are guided out of the microfluidic device using polyethylene tubing and exposed to UV light throughout 8–10 cm of the tube for approximately 5–15 seconds, depending on the applied flow rates. The microgel capsules are collected in a solution of the same composition as the outer phase (water + 2% (w/w) Tween 80).

**Microgel capsules purification.** Microgel capsules are purified by centrifugation, followed by solvent exchange. First, the synthesized microgel capsules are centrifuged at 5000 rpm for 20 minutes (Minispin, Eppendorf, Hamburg, Germany). The supernatant is replaced by fresh deionized water and centrifuged again with the same parameters. Next, the solvent is exchanged three times with isopropanol and centrifuged at 5000 rpm for 5 minutes. In a last step, isopropanol is exchanged with a 0.01 M PBS (phosphate buffered saline, pH 7.2) solution in two centrifugation steps at 5000 rpm for 15 minutes.

**Cryo-field emission scanning electron microscopy.** Structural analysis of the microgel capsules is conducted on a field emission scanning electron microscope (SU-4800, Hitachi, Tokyo, Japan). 10 μL of purified aqueous microgel capsule samples are placed on a Cryo-FESEM rivet and frozen in nitrogen cooled liquid ethane. To visualize the hollow spherical structure of the microgel capsules, a scalpel is used to break the sample on the rivet before transferring the sample to the FESEM. Water is sublimated at −80 °C for up to 25 minutes to reveal the microgel capsules structure.

**Encapsulation of FITC-labelled dextran.** To show the encapsulation of macromolecules, a 0.01% (w/w) FITC-dextran (MW = 10 kDa) solution in 1× PBS is filtered using a 1.2 μm syringe filter (Chromafil Xtra PET 120/25, MT, Düren, Germany). The FITC-dextran is applied as the inner aqueous phase during the double emulsion process to encapsulate it inside the microgel capsules. After polymerization, the microgel capsules are purified and images are taken using a fluorescence microscope at day 0 and 9 (Observer.Z1, Zeiss, Jena, Germany).

**Quantification of the FITC-labelled dextran distribution inside the microgel capsule.** The distribution of the fluorescence signal across the diameter of the microgel capsule is analyzed using the ImageJ "Plot Profile" function. Grey values per pixel and size are normalized for each microgel capsule. For day 0, 53 microgel capsules are analyzed, and for day 9, 28 are analyzed. Afterwards, the curve averages and the respective standard deviation are calculated using the OriginLab "avecurves" function.

**Rheology.** Rheology measurements of the fluidic phases applied during microfluidic experiments are conducted on a rheometer (TA Instruments HR-3 rheometer PHR3, Waters, Milford, U.S.A.), equipped with a concentric cylinder geometry. A linear flow sweep program is run from 0.1 to 100 $s^{-1}$. An increment of 10.0 $s^{-1}$ is used. Measurements are done at 25 °C. The standard sample volume is 12 mL. Viscosity values are taken at 100 $s^{-1}$.

Table 1 Liquid phases used in this work with their respective viscosities measured with a concentric cylinder geometry on a HR-3 rheometer PHR3

| Phase | Additive (% (w/w)) | Surfactant (% (w/w)) | Viscosity (mPa s) |
|---|---|---|---|
| Water | — | 2, Tween 80 | 0.94 |
| Toluene | — | 5, Span 80 | 0.66 |
| Toluene | 20, 3 kDa sPEG-OH | — | 2.21 |

## Acknowledgements

We thank Prof. Dr Martin Möller for providing the acrylate-functionalized six-armed star-shaped poly(ethylene oxide-*stat*-propylene oxide) (sPEG-A) pre-polymer, and S. Moli, N. Jansen and S. Mallmann for experimental assistance. We acknowledge funding from the European Union's Horizon 2020 research and innovation programme under Marie Skłodowska-Curie grant agreement no. 642687 and the Deutsche Forschungsgemeinschaft (DFG) within the SFB 985 "Functional Microgels and Microgel Systems" (projects C3 and B5). This work was performed in part at the Center for Chemical Polymer Technology (CPT), which was supported by the EU and the federal state of North Rhine-Westphalia (grant EFRE 30 00 883 02).

## Notes and references


1 T. M. Allen and P. R. Cullis, *Science*, 2004, **303**, 1818–1822.
2 Y. Zhang, H. F. Chan and K. W. Leong, *Adv. Drug Delivery Rev.*, 2013, **65**, 104–120.
3 D. S. Kohane, J. Y. Tse, Y. Yeo, R. Padera, M. Shubina and R. Langer, *J. Biomed. Mater. Res., Part A*, 2006, **77A**, 351–361.
4 L. De Laporte, A. des Rieux, H. M. Tuinstra, M. L. Zelivyanskaya, N. M. De Clerck, A. A. Postnov, V. Préat and L. D. Shea, *J. Biomed. Mater. Res., Part A*, 2011, **98A**, 372–382.
5 L. Sun, X. Xiong, Q. Zou, P. Ouyang, C. Burkhardt and R. Krastev, *J. Appl. Polym. Sci.*, 2017, **134**, 44425.
6 H. Lee, H. Mok, S. Lee, Y.-K. Oh and T. G. Park, *J. Controlled Release*, 2007, **119**, 245–252.
7 X.-Z. Zhang, P. Jo Lewis and C.-C. Chu, *Biomaterials*, 2005, **26**, 3299–3309.
8 P. W. Chen, R. M. Erb and A. R. Studart, *Langmuir*, 2012, **28**, 144–152.
9 J. Elisseeff, *Nat. Mater.*, 2008, **7**, 271–273.
10 A. C. Jen, M. C. Wake and A. G. Mikos, *Biotechnol. Bioeng.*, 1996, **50**, 357–364.
11 N. A. Peppas, J. Z. Hilt, A. Khademhosseini and R. Langer, *Adv. Mater.*, 2006, **18**, 1345–1360.
12 G. Zhou, Y. Lu, H. Zhang, Y. Chen, Y. Yu, J. Gao, D. Sun, G. Zhang, H. Zou and Y. Zhong, *Int. J. Nanomed.*, 2013, **8**, 877–887.
13 A. Tamura, M. Oishi and Y. Nagasaki, *Biomacromolecules*, 2009, **10**, 1818–1827.
14 S. V. Vinogradov, E. V. Batrakova and A. V. Kabanov, *Bioconjugate Chem.*, 2004, **15**, 50–60.
15 Y. Li, R. de Vries, T. Slaghek, J. Timmermans, M. A. Cohen Stuart and W. Norde, *Biomacromolecules*, 2009, **10**, 1931–1938.
16 J. Chatterjee, Y. Haik and C. Jen Chen, *Colloid Polym. Sci.*, 2003, **281**, 892–896.
17 U. Hasegawa, S.-I. M. Nomura, S. C. Kaul, T. Hirano and K. Akiyoshi, *Biochem. Biophys. Res. Commun.*, 2005, **331**, 917–921.
18 J. C. Rose, M. Cámara-Torres, K. Rahimi, J. Köhler, M. Möller and L. De Laporte, *Nano Lett.*, 2017, DOI: 10.1021/acs.nanolett.7b01123.
19 Y. Hu, W. Liu and F. Wu, *RSC Adv.*, 2017, **7**, 10333–10344.
20 S. Uthaman, S. Zheng, J. Han, Y. J. Choi, S. Cho, V. D. Nguyen, J.-O. Park, S.-H. Park, J.-J. Min, S. Park and I.-K. Park, *Adv. Healthcare Mater.*, 2016, **5**, 288–295.
21 T. Trongsatitkul and B. M. Budhlall, *Polym. Chem.*, 2013, **4**, 1502–1516.
22 A. Arun and B. S. R. Reddy, *Biomaterials*, 2005, **26**, 1185–1193.
23 B. J. Kong, A. Kim and S. N. Park, *Carbohydr. Polym.*, 2016, **147**, 473–481.
24 J. Li and D. J. Mooney, *Nat. Rev. Mater.*, 2016, **1**, 16071.
25 H. Kawaguchi, *Polym. Int.*, 2014, **63**, 925–932.
26 B. R. Saunders, N. Laajam, E. Daly, S. Teow, X. Hu and R. Stepto, *Adv. Colloid Interface Sci.*, 2009, **147–148**, 251–262.
27 L. Bromberg, M. Temchenko and T. A. Hatton, *Langmuir*, 2002, **18**, 4944–4952.
28 D. Chong, X. Liu, H. Ma, G. Huang, Y. L. Han, X. Cui, J. Yan and F. Xu, *Microfluid. Nanofluid.*, 2015, **19**, 1071–1090.
29 W. Richtering, I. I. Potemkin, A. A. Rudov, G. Sellge and C. Trautwein, *Nanomedicine*, 2016, **11**, 2879–2883.
30 A. J. Schmid, J. Dubbert, A. A. Rudov, J. S. Pedersen, P. Lindner, M. Karg, I. I. Potemkin and W. Richtering, *Sci. Rep.*, 2016, **6**, 22736.
31 T. Femmer, A. Jans, R. Eswein, N. Anwar, M. Moeller, M. Wessling and A. J. C. Kuehne, *ACS Appl. Mater. Interfaces*, 2015, **7**, 12635–12638.
32 S. Seiffert, M. B. Romanowsky and D. A. Weitz, *Langmuir*, 2010, **26**, 14842–14847.
33 S. Seiffert, J. Thiele, A. R. Abate and D. A. Weitz, *J. Am. Chem. Soc.*, 2010, **132**, 6606–6609.
34 T. Rossow, J. A. Heyman, A. J. Ehrlicher, A. Langhoff, D. A. Weitz, R. Haag and S. Seiffert, *J. Am. Chem. Soc.*, 2012, **134**, 4983–4989.
35 A. Jans, R. R. Rosencrantz, A. D. Mandic, N. Anwar, S. Boesveld, C. Trautwein, M. Moeller, G. Sellge, L. Elling and A. J. C. Kuehne, *Biomacromolecules*, 2017, **18**(5), 1460–1465.
36 J. K. Nunes, S. S. H. Tsai, J. Wan and H. A. Stone, *J. Phys. D: Appl. Phys.*, 2013, **46**, 114002.
37 S. Seiffert and D. A. Weitz, *Soft Matter*, 2010, **6**, 3184–3190.
38 A. S. Utada, L. Y. Chu, A. Fernandez-Nieves, D. R. Link, C. Holtze and D. A. Weitz, *MRS Bull.*, 2007, **32**, 702–708.
39 H. Bysell, R. Månsson, P. Hansson and M. Malmsten, *Adv. Drug Delivery Rev.*, 2011, **63**, 1172–1185.
40 C. D. A. L. Chaves, A. L. Machado, I. Z. Carlos, E. T. Giampaolo, A. C. Pavarina and C. E. Vergani, *Dent. Mater.*, 2010, **26**, 1017–1023.
41 M. Armaka, E. Papanikolaou, A. Sivropoulou and M. Arsenakis, *Antiviral Res.*, 1999, **43**, 79–92.
42 J. Pessi, H. A. Santos, I. Miroshnyk, J. Yliruusi, D. A. Weitz and S. Mirza, *Int. J. Pharm.*, 2014, **472**, 82–87.
43 J. K. Tessmar and A. M. Göpferich, *Adv. Drug Delivery Rev.*, 2007, **59**, 274–291.
44 M. B. Browning, T. Wilems, M. Hahn and E. Cosgriff-Hernandez, *J. Biomed. Mater. Res., Part A*, 2011, **98A**, 268–273.
45 T. R. Hoare and D. S. Kohane, *Polymer*, 2008, **49**, 1993–2007.
46 M. Sheikhpour, L. Barani and A. Kasaeian, *J. Controlled Release*, 2017, **253**, 97–109.
47 I. S. Kikuchi, R. S. Galante, K. Dua, V. R. Malipeddi, R. Awasthi, D. D. Ghisleni and T. de Jesus Andreoli Pinto, *Curr. Drug Delivery*, 2016, **13**, 1–9.
48 M. K. Nguyen and E. Alsberg, *Prog. Polym. Sci.*, 2014, **39**, 1235–1265.


 

49 S. P. Zustiak and J. B. Leach, *Biomacromolecules*, 2010, **11**, 1348–1357.
50 M. B. Browning, S. N. Cereceres, P. T. Luong and E. M. Cosgriff-Hernandez, *J. Biomed. Mater. Res., Part A*, 2014, **102**, 4244–4251.
51 A. S. Utada, E. Lorenceau, D. R. Link, P. D. Kaplan, H. A. Stone and D. A. Weitz, *Science*, 2005, **308**, 537.
52 P. W. Chen, J. Brignoli and A. R. Studart, *Polymer*, 2014, **55**, 6837–6843.
53 A. S. Hoffman, *Adv. Drug Delivery Rev.*, 2002, **54**, 3–12.
54 TdB Consultancy, FITC dextran product sheet, http://www.tdbcons.com/images/pdf/fitcdextran2.pdf (accessed December 2016).
55 M. C. Lensen, P. Mela, A. Mourran, J. Groll, J. Heuts, H. Rong and M. Möller, *Langmuir*, 2007, **23**, 7841–7846.